Supplementary Information (SI) for ChemComm.

Electronic Supporting Information

Effect of pressure and temperature on the structure and optical properties of two-dimensional lead iodide perovskites

Viktoriia Drushliak[a] and Marek Szafrański*[a]

[a]*Faculty of Physics and Astronomy, Adam Mickiewicz University, Uniwersytetu Poznańskiego 2,*
61-614 Poznań, Poland

**Corresponding author: Marek Szafrański, e-mail: masza@amu.edu.pl*

Materials and Methods

Chemicals and reagents were purchased and used for syntheses without further purification: guanidinium carbonate (99%, Sigma-Aldrich), caesium carbonate (99%, Sigma-Aldrich), lead(II) iodide (99%, Acros Organics) and hydroiodic acid (57% in water, stabilised with 1.5% hypophosphorous acid, Alfa Aestar). By the reaction of carbonates with hydroiodic acid, caesium iodide and guanidinium iodide were obtained and used as the substrates for further syntheses.

$[C(NH_2)_3]_2PbI_4$ was synthesised in a non-stoichiometric solution containing an excess of $C(NH_2)_3I$. 10 mmol of $C(NH_2)_3I$ was dissolved in hot water (~80°C) acidified with HI, and then the hot solution of 3 mmol of PbI_2 dissolved in 10 ml of HI was added drop by drop with constant stirring. Slow cooling of the solution to room temperature resulted in crystallisation of yellow platelets that were harvested, washed with diethyl ether, and dried. The yield obtained, determined in relation to PbI_2, was approximately 60%.

$CsC(NH_2)_3PbI_4$ was obtained from the hot acid solution using the procedure described by Nazarenko *et al.*[1] 2 mmol of PbI_2, 2 mmol of CsI, and 8 mmol of $C(NH_2)_3I$ were dissolved in 13 ml of HI. The solution was heated and stirred until dissolution of all substrates and then slowly cooled. During several hours of cooling from ~80°C to room temperature, red crystals precipitated. Crystals were harvested, washed with diethyl ether, and dried. The yield of approximately 65% was estimated in relation to PbI_2.

Both materials obtained have been identified by single-crystal X-ray diffraction.

Thermal properties were studied by differential scanning calorimetry (DSC) with the Q2000 calorimeter (TA Instruments), and by thermogravimetric analysis (TGA) using the TGA Q50 instrument (TA Instruments). Both experiments were carried out on powdered samples with a temperature change rate of 10 K min^{-1}.

Single-crystal X-ray diffraction (SCXRD) experiments were performed as a function of temperature and pressure using a four-circle Oxford Diffraction Gemini A Ultra diffractometer operating with graphite-monochromated Mo Kα radiation ($\lambda = 0.71073$ Å). Data were collected and processed using the CrysAlisPro software.[2] Temperature-dependent measurements were carried out in the range from 200 to 380 K. The temperature of the crystals was controlled with an accuracy ± 0.1 K using a Cryostream Plus Cooler (Oxford Cryosystems).

High-pressur experiments were conducted using a modified Merrill-Bassett diamond anvil cell (DAC)[3] equipped with symmetric diamond anvils (culet diameter 0.8 mm) supported on steel discs with conical windows. A steel foil of 250 µm thickness with spark-eroded hole of an approximate diameter of 360 µm was used as a gasket. A selected single crystal with a ruby chip as the pressure calibrant and Daphne oil 7575 as the pressure transmitting medium was loaded into the pressure chamber. The pressure was calibrated before and after each measurement, using the ruby fluorescence method[4] with an accuracy of ± 0.03 GPa. The DAC was centred by the gasket-shadowing method.[5]

Structures were solved and refined using the SHELX and Olex2 software.[6,7] Crystallographic information files (CIFs) for the $[C(NH_2)_3]_2PbI_4$ structures determined under pressure (2428383–2428386) and for the $CsC(NH_2)_3PbI_4$ structures determined at different temperatures and under pressures (2428387–2428400) have been deposited with the Cambridge Crystallographic Data Centre.

Optical absorption spectra were recorded using a Jasco MSV-5100 microscopic spectrophotometer. The absorbance was measured from a small sample area with a diameter of 30 µm at a scan speed of 200 nm min^{-1} and a spectral bandwidth of 5 nm, in the range from 500 to 800 nm. Temperature measurements were made over a range between 79 K and 458 K using a Linkam THMSE600 heating and freezing stage. High-pressure measurements were conducted at room temperature using a DAC equipped with low-fluorescence type IIa diamond anvils. The pressure calibration and hydrostatic liquid were analogous as in the case of the SCXRD experiments.

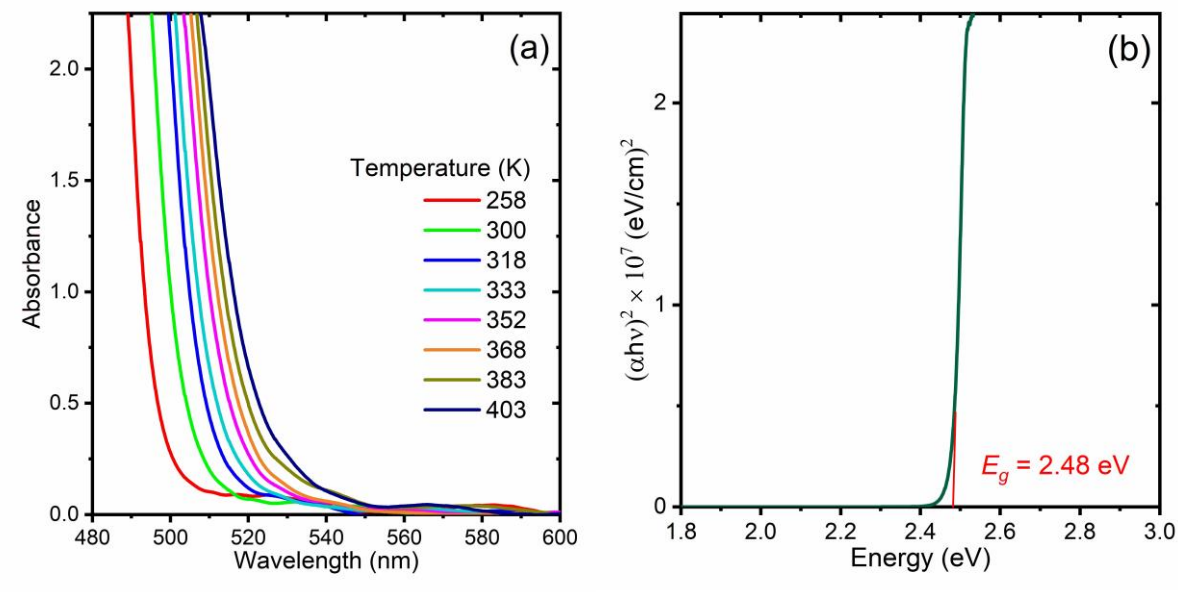

Figure S1 (a) Selected optical absorbance spectra measured for a single-crystal plate of $[C(NH_2)_3]_2PbI_4$ at different temperatures. (b) Tauc plot[8] and energy gap determined from the absorption spectrum measured at 300 K.

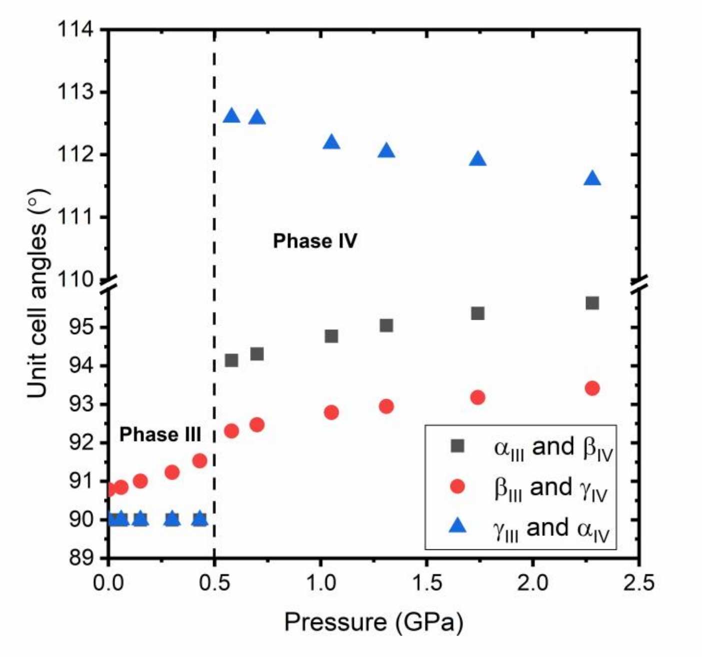

Figure S2 Pressure dependence of the unit-cell angles of $[C(NH_2)_3]_2PbI_4$.

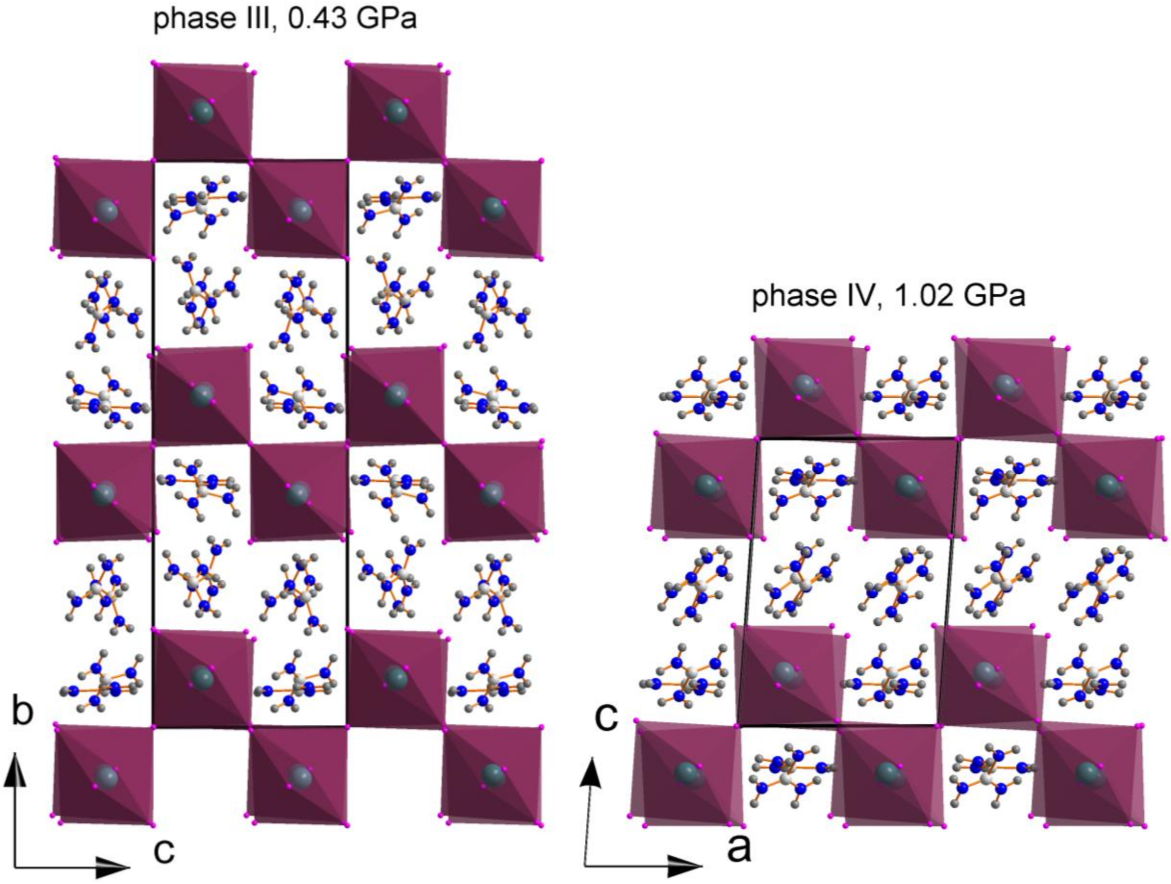

Figure S3 Crystal structure of $[C(NH_2)_3]_2PbI_4$ in phase III at 0.43 GPa and in phase IV at 1.02 GPa.

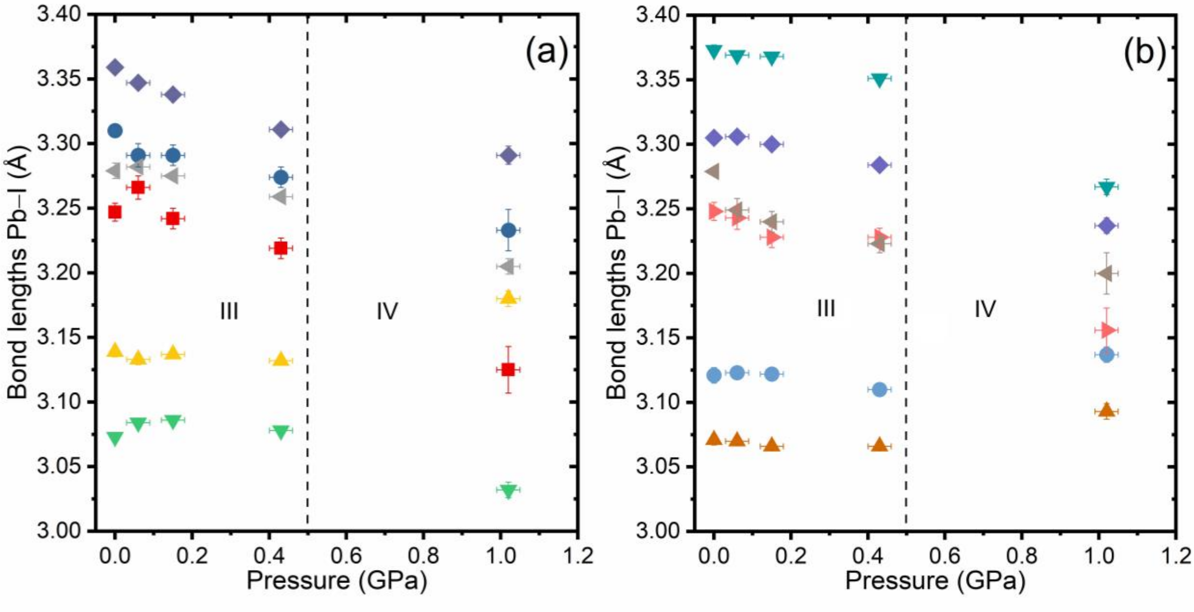

Figure S4 Pressure dependence of the Pb–I bond lengths in the two symmetry-independent PbI_6 octahedra plotted in parts (a) and (b), respectively, in phases III and IV of $[C(NH_2)_3]_2PbI_4$.

Crystal structure description and pressure-induced structural changes in $[C(NH_2)_3]_2PbI_4$

At room temperature $[C(NH_2)_3]_2PbI_4$ crystallises in phase III of the space group $P2_1/n$.[9] The structure is formed of double layers of corner-sharing PbI_6 octahedra, arranged perpendicular to *b* (Fig. S3). In these perovskite layers, every second octahedron is missing, which creates a space for guanidinium cations. Because the size of $C(NH_2)_3^+$ is somewhat incompatible with the size of the perovskite cage the adjacent PbI_6 octahedra are alternately tilted relative to the *a*-axis, to accommodate the cation. Guanidinium cations also occupy space between the layers, forming barriers for charge carriers. The cations in both sites are linked to the inorganic framework through weak N–H···I hydrogen bonds.

Under pressure, phase III of $[C(NH_2)_3]_2PbI_4$ is stable in the pressure range to 0.5 GPa, where the crystal transforms to the triclinic phase IV of the space group $P\overline{1}$. In phase IV the lattice parameter *c*, corresponding to *b* in phase III, is halved, as seen in Fig. 3. The change of symmetry from monoclinic to triclinic defines this transition as ferroelastic, which justifies the appearance of ferroelastic domains. Crystal twinning hindered the XRD experiments, but nonetheless a phase IV structural model was refined from the data collected at 1.02 GPa. In the structure of phases III and IV, there are two symmetry-independent PbI_6 octahedra, both substantially distorted from an ideal octahedral symmetry, as reflected in the Pb–I bond lengths plotted in Fig. S4. With increasing pressure in phase III these bonds progressively contract. To track the distortion of the octahedra as a function of pressure, the octahedral distortion parameter *Δd* was calculated using the following formula:

$$\Delta d = \frac{1}{6}\sum_{n=1}^{6}\left[\frac{d_n - d}{d}\right]^2,$$

where d is the average Pb–I distance, and d_n are the individual Pb–I distances. The results in Fig. S5 show a substantial reduction in *d* with increasing pressure, indicating a significant reduction in the distortion of the octahedra. This distortion is further reduced after the transition to phase IV.

Figure S6 shows the pressure dependence of the Pb–I–Pb angles which reflect the PbI_6 octahedra tilts. As seen, these tilts increase in phase III up to the transition point where the substantial changes take place. The straightening of the two smallest Pb–I–Pb angles is responsible for the abrupt narrowing of the energy gap at the transition point at 0.5 GPa.

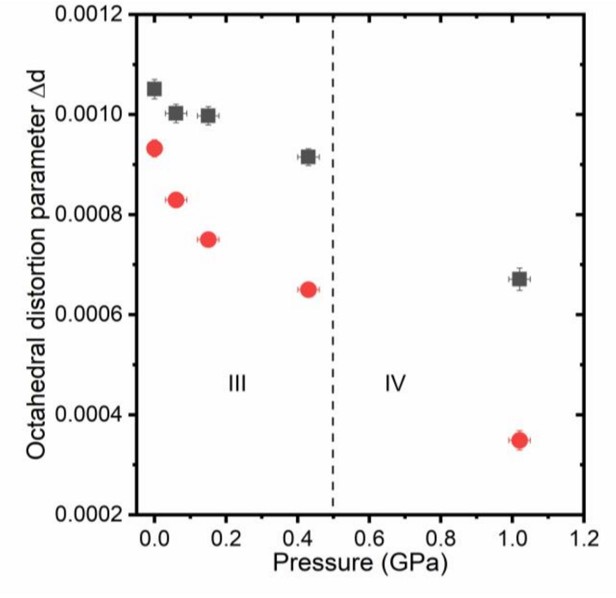

Figure S5 Octahedral distortion parameter Δd plotted as a function of pressure for two symmetry-independent PbI_6 octahedra present in the structure of phases III and IV of $[C(NH_2)_3]_2PbI_4$.

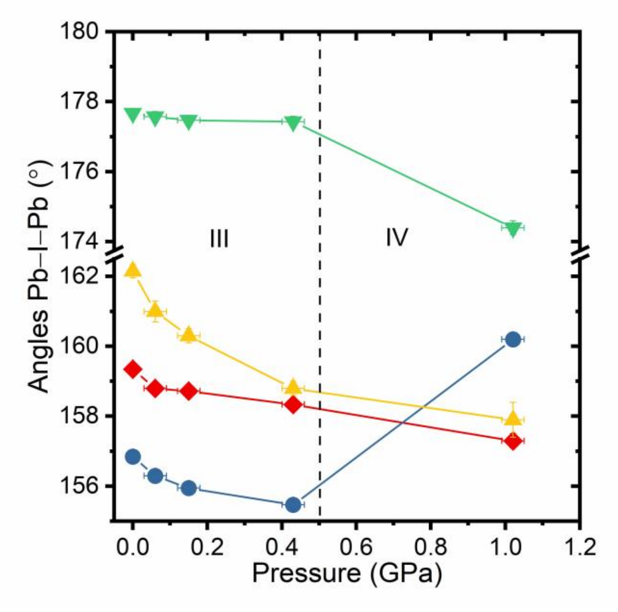

Figure S6 Pb–I–Pb angles plotted in phases III and IV of $[C(NH_2)_3]_2PbI_4$ as a function of pressure.

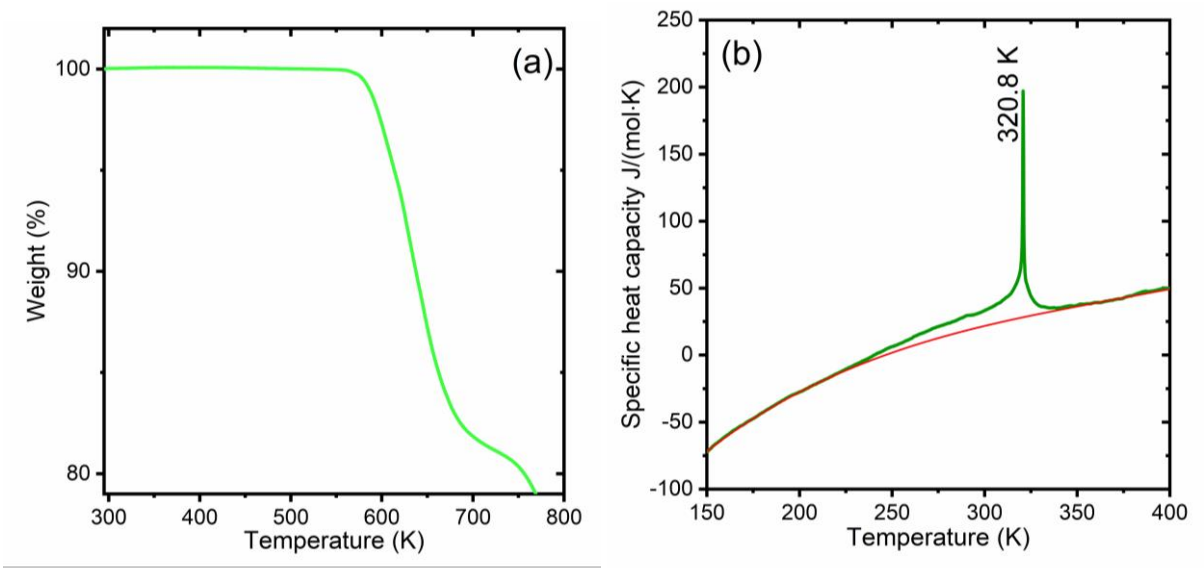

Figure S7 (a) Thermogravimetric analysis of the powdered $CsC(NH_2)_3PbI_4$ crystals and (b) temperature dependence of the specific heat capacity. The red line in (b) marks the baseline used for the entropy change calculation.

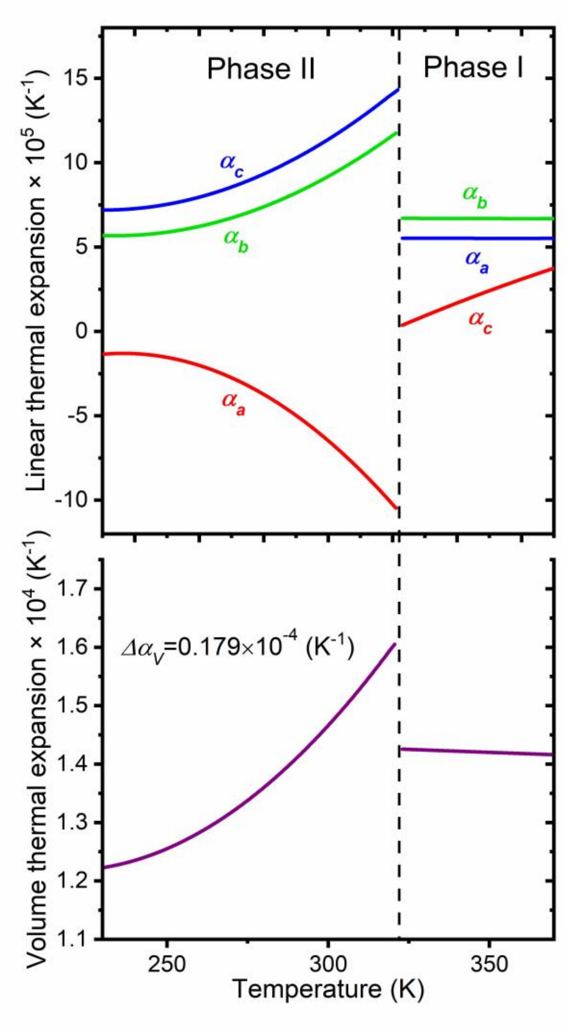

Figure S8 Temperature dependence of the linear and volumetric thermal expansion coefficients of $CsC(NH_2)_3PbI_4$.

Crystal structures in phases I and II of $CsC(NH_2)_3PbI_4$

At room temperature and under atmospheric pressure $CsC(NH_2)_3PbI_4$ crystallises in the space group *Pnnm*.[1] The corner-linked PbI_6 octahedra form single layers perpendicular to the *a*-axis (Fig. S9, left panels). The octahedra are distorted from an ideal octahedral symmetry and alternately tilted in opposite directions relative to the plane (100) and also to the plane (001). Due to the octahedra tilts, two kinds of cavities of different size are formed within the inorganic framework. The small and large cavities are occupied by the cations Cs^+ and $C(NH_2)_3^+$, respectively.

The crystal undergoes a second-order phase transition at 320.8 K to the orthorhombic phase I of the space group *Imma*. As shown in Fig. S9 (right panels) in phase I the iodine atoms, shared by PbI_6 octahedra along the *a*-axis (*a* in phase I corresponds to *c* in phase II), are disordered between two sites. Moreover, the alternating tilts of the PbI_6 octahedra relative to the plane (001) in phase II disappear in phase I, resulting in a halved lattice parameter *b*.

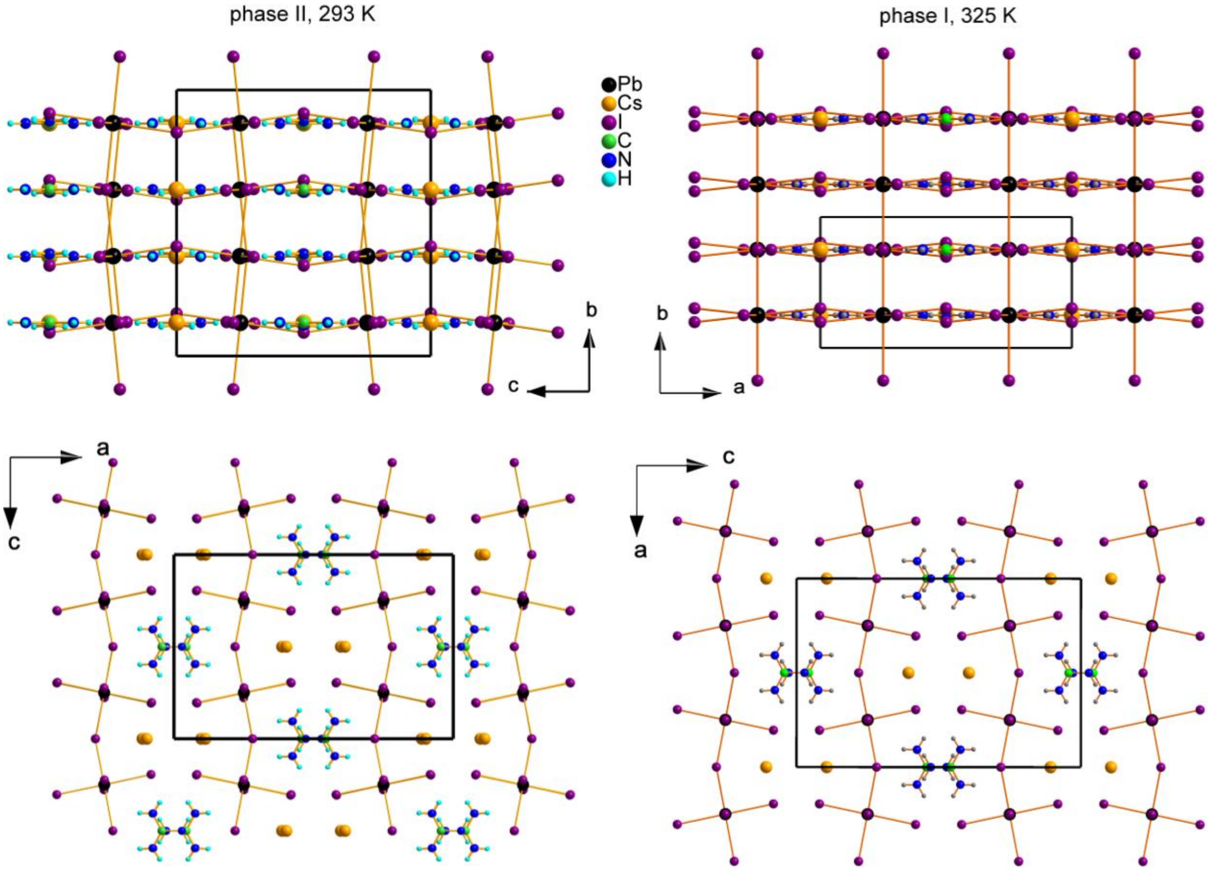

Figure S9 Crystal structures of $CsC(NH_2)_3PbI_4$ in phases II (left) and I (right) viewed along the equivalent directions.

Pressure-induced isostructural phase transition in $CsC(NH_2)_3PbI_4$ at 4.5 GPa

Under pressure at 4.5 GPa, $CsC(NH_2)_3PbI_4$ undergoes a structural phase transition, but in the high-pressure phase III the crystal retains the same symmetry of the space group *Pnnm* as in phase II. The transition is associated with jumpwise changes in the lattice parameters and it also significantly affects the Pb–I bond lengths and Pb–I–Pb angles. The pressure dependence of the octahedral distortion parameter *Δd* is shown in Fig. S10. In phase II, with increasing pressure, the distortion of the PbI_6 octahedron initially changes only slightly but increases significantly as the transition approaches. A jumpwise decrease in *Δd* at the transition point indicates that under pressure in phase III the octahedra become more symmetric.

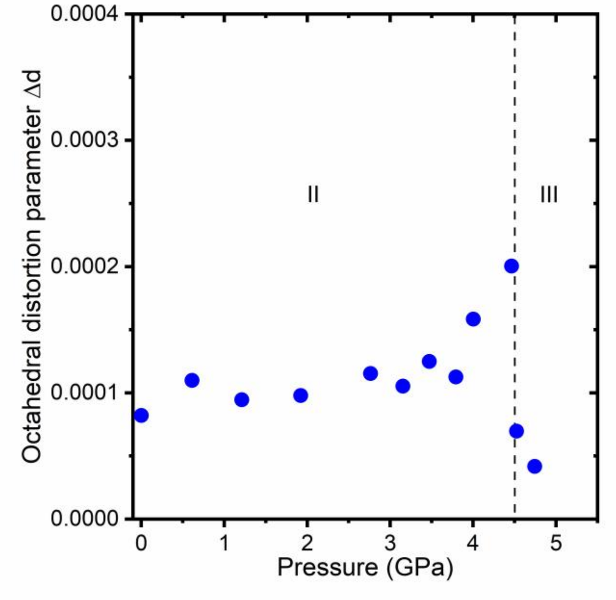

Figure S10 Octahedral distortion parameter Δd derived from the structural models of $CsC(NH_2)_3PbI_4$ obtained at various pressures.

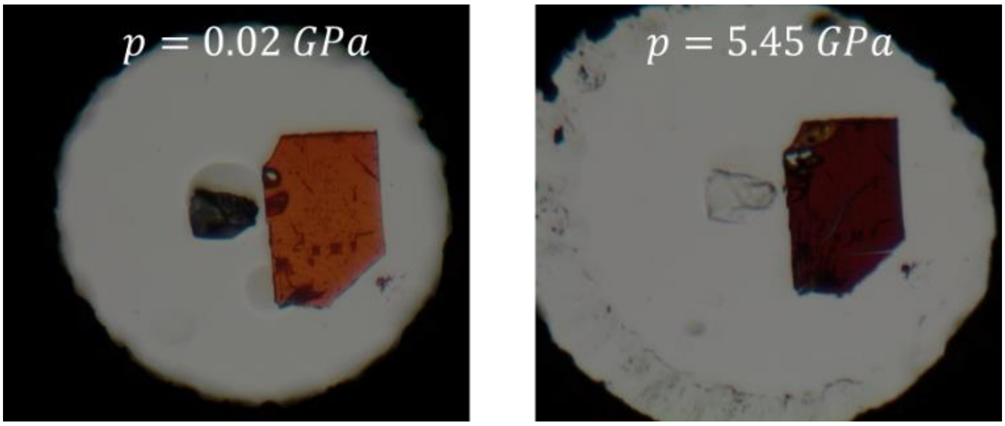

Figure S11 Photos of $CsC[(NH_2)_3]PbI_4$ showing the color change of the crystal under pressure.

Table S1. Selected crystallographic and refinement data for the structures of $[C(NH_2)_3]_2PbI_4$.

Crystal formula	$[C(NH_2)_3]_2PbI_4$		
Color	yellow		
Pressure (GPa)	0.15	0.43	1.02
Crystal system	Monoclinic		Triclinic
Space group	$P2_1/n$		$P\overline{1}$
Z	8		4
Crystal size (mm)	0.12 × 0.06 × 0.03		
a (Å)	12.742(6)	12.673(4)	9.1051(7)
b (Å)	26.9140(17)	26.7036(12)	12.466(4)
c (Å)	9.2472(4)	9.1630(3)	14.0938(16)
α (°)	90	90	67.82(2)
β (°)	88.992(11)	88.468(8)	85.226(7)
γ (°)	90	90	87.169(14)
Volume ($Å^3$)	3170.9(14)	3099.7(10)	1475.9(6)
ρ (g cm^{-3})	3.498	3.578	3.758
μ (mm^{-1})	18.410	18.832	19.776
No. of measured, independent and observed [$I > 2\sigma(I)$] refl.	14294, 1864, 1094	13873, 1836, 1137	1668, 1668, 890
R_{int}	0.0927	0.0821	0.0945
R_1 [$I > 2\sigma(I)$], $R_1(all)$	0.061, 0.131	0.057, 0.124	0.062, 0.127
wR_2 [$I > 2\sigma(I)$], $wR_2(all)$	0.111, 0.132	0.115, 0.143	0.159, 0.175
GOF	1.099	1.086	1.097

Table S2. Selected crystallographic and refinement data for the structures of $CsC(NH_2)_3PbI_4$.

Crystal formula	$CsC(NH_2)_3PbI_4$		
Color	red		
Pressure (GPa)	0.0001	2.76	4.52
Crystal system Space group Z	Orthorhombic *Pnnm* 8		
Crystal size (mm)	0.18 × 0.05 × 0.02	0.18 × 0.14 × 0.04	
a (Å) *b* (Å) *c* (Å)	18.5595(4) 12.7464(3) 12.2365(3)	17.914(8) 12.0823(4) 11.6499(4)	17.475(19) 11.8768(5) 11.5309(4)
Volume (Å^3)	2894.76(12)	2521.5(11)	2393(3)
ρ (g cm^{-3})	4.166	4.783	5.039
μ (mm^{-1})	22.627	25.976	27.369
No. of measured, independent and observed [$I > 2\sigma(I)$] reflections	15731, 3543, 2039	10382, 971, 613	9315, 613, 406
R_{int}	0.0489	0.0681	0.0899
R_1 [$I > 2\sigma(I)$], $R_1(all)$	0.046, 0.083	0.04, 0.07	0.077, 0.106
wR_2 [$I > 2\sigma(I)$], $wR_2(all)$	0.121, 0.156	0.099, 0.116	0.178, 0.197
GOF	1.105	1.194	1.056

References

1 O. Nazarenko, M. R. Kotyrba, M. Wörle, E. Cuervo-Reyes, S. Yakunin, M. Kovalenko, *Inorg. Chem*. 2017, **56**, 11552–11564.

2 Agilent Technologies. CrysAlisPro: Data Collection and Processing Software for X-Ray Diffractometers, Santa Clara, CA, 2010.

3 L. Merrill and W. A. Bassett, *Rev. Sci. Instrum*., 1974, **45**, 290–294.

4 R. A. Forman, G. J. Piermarini, J. D. Barnett and S. Block, *Science* 1972, **176**, 284–285.

5 A. Katrusiak, *Z. Kristallogr. Cryst. Mater*., 2004, **219**, 461–467.

6 Sheldrick G.M., *Acta Crystallogr. A*, 2008, *64*, 112–122.

7 O. V. Dolomanov, L. J. Bourhis, R. J. Gildea, J. A. K. Howard and H. Puschmann, J. *Appl. Crystallogr.*, 2009, **42**, 339–341.

8 J. Tauc, R. Grigorovici and A. Vancu, *Phys. Status Solidi B*, 1966, **15**, 627–637.

9 M. Szafrański and A. Katrusiak, *Phys. Rev. B*, 2000, **61**, 1026–1035.